

Analysis of the generation mechanism of the S-shaped *J-V* curves of MoS_2/Si-based solar cells

He-Ju Xu(许贺菊), Li-Tao Xin(辛利桃), Dong-Qiang Chen(陈东强),Ri-Dong Cong(丛日东), and Wei Yu(于威)
Citation: Chin. Phys. B, 2022, 31 (**3**): 038503. DOI: 10.1088/1674-1056/ac1b80
Journal homepage: http://cpb.iphy.ac.cn; http://iopscience.iop.org/cpb
What follows is a list of articles you may be interested in

A 4H-SiC merged P-I-N Schottky with floating back-to-back diode

Wei-Zhong Chen(陈伟中), Hai-Feng Qin(秦海峰), Feng Xu(许峰), Li-Xiang Wang(王礼祥), Yi Huang(黄义), and Zheng-Sheng Han(韩郑生)
Chin. Phys. B, 2022, 31 (**2**): 028503. DOI: 10.1088/1674-1056/ac0e23

A 3D SiC MOSFET with poly-silicon/SiC heterojunction diode

Sheng-Long Ran(冉胜龙), Zhi-Yong Huang(黄智勇), Sheng-Dong Hu(胡盛东), Han Yang(杨晗), Jie Jiang(江洁), and Du Zhou(周读)
Chin. Phys. B, 2022, 31 (**1**): 018504. DOI: 10.1088/1674-1056/ac0038

Metal halide perovskite photodetectors: Material featuresand device engineering

Ye Wang(王烨), Meng-Lei Gao(高孟磊), Jin-Liang Wu(吴金良), Xing-Wang Zhang(张兴旺)
Chin. Phys. B, 2019, 28 (**1**): 018502. DOI: 10.1088/1674-1056/28/1/018502

Performance enhancement of ZnO nanowires/PbS quantum dot depleted bulk heterojunction solar cells with an ultrathin Al_2O_3 interlayer

Shuaipu Zang(臧帅普), Yinglin Wang(王莹琳), Meiying Li(李美莹), Wei Su(苏蔚), Meiqi An(安美琦), Xintong Zhang(张昕彤), Yichun Liu(刘益春)
Chin. Phys. B, 2018, 27 (**1**): 018503. DOI: 10.1088/1674-1056/27/1/018503

Organic photovoltaic cells with copper (Ⅱ) tetra-methyl substituted phthalocyanine

Xu Zong-Xiang, Roy V. A. L.
Chin. Phys. B, 2013, 22 (**12**): 128505. DOI: 10.1088/1674-1056/22/12/128505

Analysis of the generation mechanism of the S-shaped J–V curves of MoS_2/Si-based solar cells

He-Ju Xu(许贺菊)[1,†], Li-Tao Xin(辛利桃)[2], Dong-Qiang Chen(陈东强)[2], Ri-Dong Cong(丛日东)[2,‡], and Wei Yu(于威)[2,§]

[1] *College of Science, North China University of Science and Technology, Tangshan* 063009, *China*
[2] *College of Physics Science and Technology, Hebei University, Baoding* 071002, *China*

(Received 13 February 2021; revised manuscript received 2 August 2021; accepted manuscript online 7 August 2021)

Amorphous–microcrystalline MoS_2 thin films are fabricated using the sol-gel method to produce MoS_2/Si-based solar cells. The generation mechanisms of the S-shaped current density–voltage (J–V) curves of the solar cells are analyzed. To improve the performance of the solar cells and address the problem of the S-shaped J–V curve, a MoS_2 film and a p^+ layer are introduced into the front and back interfaces of the solar cell, respectively, which leads to the formation of a p–n junction between the p-Si and the MoS_2 film as well as ohmic contacts between the MoS_2 film and the ITO, improving the S-shaped J–V curve. As a result of the high doping characteristics and the high work function of the p^+ layer, a high–low junction is formed between the p^+ and p layers along with ohmic contacts between the p^+ layer and the Ag electrode. Consequently, the S-shaped J–V curve is eliminated, and a significantly higher current density is achieved at a high voltage. The device exhibits ideal p–n junction rectification characteristics and achieves a high power-conversion efficiency (CE) of 7.55%. The findings of this study may improve the application of MoS_2 thin films in silicon-based solar cells, which are expected to be widely used in various silicon-based electronic and optical devices.

Keywords: MoS_2/Si-based solar cell, S-shaped J–V curve, power conversion efficiency, p^+ layer

PACS: 85.30.–z, 81.10.–h **DOI:** 10.1088/1674-1056/ac1b80

1. Introduction

Transition-metal dichalcogenides (TMDs) have attracted increasing attention due to their rich electrical and optical properties. As typical TMD materials, MoS_2 films have strong optical absorption characteristics and high carrier mobility, and exhibit unique photoelectric characteristics that make them suitable for use in MoS_2/Si-based solar cells.

In previous studies,[1,2] MoS_2 films were fabricated via the sol-gel method, and MoS_2/Si-based solar cells were successfully prepared. The introduction of the MoS_2 film improved the performance of the solar cells and enabled them to obtain a conversion efficiency of 4.6%. However, an S-shaped J–V curve was observed, which exhibited nonideal p–n junction rectification characteristics. The S-shaped J–V curve attenuates the output characteristic parameters, such as the open circuit voltage (V_{OC}), the short circuit current density (J_{SC}), and the fill factor (FF), which affects the conversion efficiency of the solar sell. Therefore, studying the generation mechanism of the S-shaped J–V curve and improving the S-shape are beneficial for improving the conversion efficiency. Research into the generation mechanism of the S-shaped J–V curve has attracted widespread attention.[3–9] Carabe *et al.*[3] proposed that non-ohmic contacts at the back interface of the heterojunction cause the formation of an S-shaped J–V curve. Wang *et al.*[4] further analyzed the S-shaped J–V curve generation mechanism of the non-ohmic contacts at the back of the heterojunction and reported that the size of the back contact barrier influences the formation of the S-shaped J–V curve. The physical correlation between the electrical property degradation of the hole-selective layer and the generation of an S-shaped J–V curve in an inverted organic solar cell was analyzed by René Kogler *et al.*[5] Liu *et al.*[9] proposed that interface engineering was crucial for the development of efficient solar cells and consequently, the power conversion efficiency was enhanced from 7.5% to 15.5%.

In this study, a MoS_2 film is introduced into the front interface of the solar cell to analyze the generation mechanism of the S-shaped J–V curve, and a p–n heterojunction is formed, enhancing the V_{OC} and FF of the solar cell and improving the S-shape of the J–V curve. The introduction of a p^+ layer into the back interface of the solar cell reduces the back contact barrier of the solar cell and eliminates the S-shape of the J–V curve, achieving high power-conversion efficiency.

2. Experiment

2.1. Preparation

Figure 1(a) shows a structural diagram of a primitive solar cell, which is referred to as sample 1. Figures 1(b) and 1(c) show diagrams of a solar cell with an MoS_2 film at the front

†Corresponding author. E-mail: xuheju@ncst.edu.cn
‡Corresponding author. E-mail: congrd@hbu.edu.cn
§Corresponding author. E-mail: yuwei@hbu.edu.cn

© 2022 Chinese Physical Society and IOP Publishing Ltd

interface and a cell with a MoS_2 film at the front interface and a p^+ layer at the back interface, called sample 2 and sample 3, respectively. The details of the preparation of the MoS_2 thin films, ITO, and Ag electrodes were presented in our previous work.[1] A p^+ layer was prepared in the chamber of a PECVD deposition system at a deposition temperature of 300 °C, a power of 21 W, and a working pressure of 253.3 Pa. The flow rates of SiH_4, H_2, CO_2, and B_2H_6 were 1.3 sccm, 201 sccm, 1.0 sccm, and 0.54 sccm, respectively, and the deposition time was 20 min.

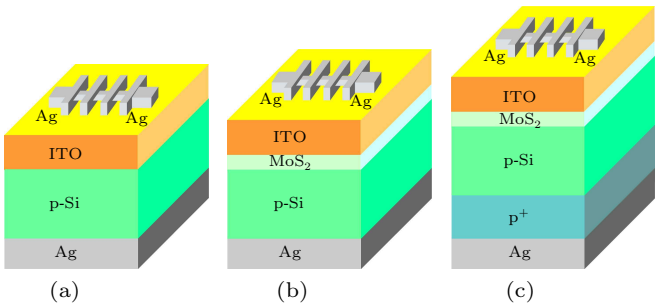


Fig. 1. Structure diagram of (a) sample 1, (b) sample 2, and (c) sample 3.

A scanning electron microscopy (SEM) image of the cross section of sample 3 is shown in Fig. 2, in which the presence of Si, ITO, and Ag can clearly be identified. However, the thickness of the MoS_2 layer is less than 10 nm, and we could not confirm the presence of the MoS_2 layer using the SEM cross-sectional image.

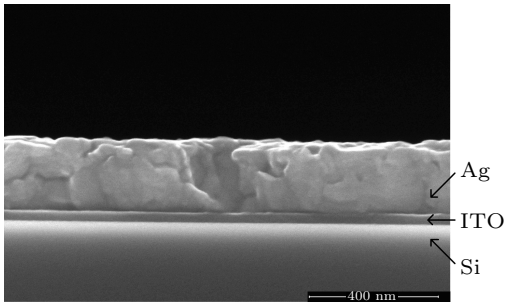


Fig. 2. SEM image of the cross section of sample 3.

2.2. Characterization

A semiconductor device parameter analyzer (Agilent B1500A) was used at room temperature to measure the *J*–*V* curves in the dark and under AM 1.5 illumination, as well as the capacitance–voltage (*C*–*V*) curves. The external quantum efficiency (EQE) was measured using the equipment described in our previous work.[1]

3. Results and discussion

The structure and quality of the MoS_2 film were analyzed via XRD, Raman spectroscopy, and XPS measurements in our previous work.[1] The results indicate that the MoS_2 film was successfully prepared. Figures 3(a) and 3(b) present the *J*–*V* curves of samples 1–3 under AM 1.5 illumination and dark conditions. The photovoltaic parameters of the three samples are listed in Table 1 and it can be observed that the photovoltaic performances of the three samples gradually improve. V_{OC} first increases from 116 mV to 236 mV, and then to 328 mV; J_{SC} first increases from 31.73 mA·cm^{-2} to 34.49 mA·cm^{-2}, and then to 37.21 mA·cm^{-2}; the FF first increases from 0.30 to 0.57, and then to 0.62; finally, the CE first increases from 1.1% to 4.6% and then to 7.55%. A p–n heterojunction is formed in the sample 2 due to the introduction of MoS_2, producing a larger built-in electric field and a wider depletion region. The photo-excited carriers are effectively separated,[10] resulting in an increase in V_{OC} and J_{SC}. The serial ohmic loss and the ohmic shunt decrease due to the passivation effect of the MoS_2 film on the interface and the high conductivity of the p^+ layer, which improves the V_{OC}, J_{SC}, and FF. The shape of the *J*–*V* curve also changes. The *J*–*V* curves of samples 1 and 2 are both S-shaped; however, the shape of the *J*–*V* curve of sample 2 is clearly improved, while the S-shape of the *J*–*V* curve of sample 3 is eliminated and is similar to that of an ideal diode.

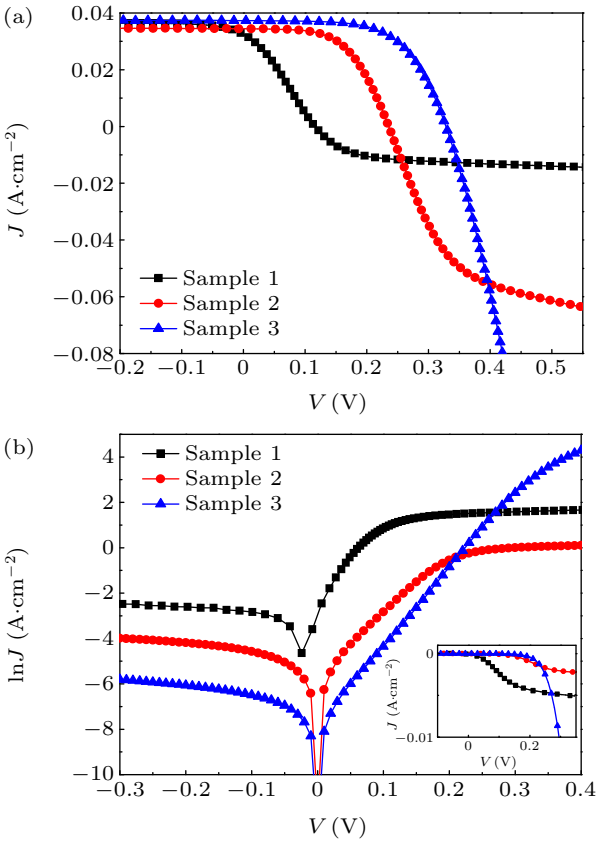


Fig. 3. (a) The *J*–*V* curves under AM 1.5 illumination, (b) ln*J*–*V* curves, the inset are *J*–*V* curves under dark conditions for samples 1–3.

The ideal factor, *n*, is extracted from Fig. 3(b), as shown in Table 1.[1] The ideal factors of samples 1–3 are 1.63, 1.45, and 1.10, respectively, implying an improvement in the performance of the samples due to the introduction of the MoS_2 film and the p^+ layer.

Table 1. Photovoltaic parameters of samples 1–3.

Sample	V_{OC} (mV)	J_{SC} (mA·cm^{-2})	FF	CE$_f$ (%)	R_s (Ω)	R_{sh} (Ω)	n	W (nm)	N_b (cm^{-2})
Sample 1	116	31.73	0.30	1.1	9.85	40	1.63	182	2.97×10^{16}
Sample 2	236	34.49	0.57	4.6	1.59	68	1.45	332	1.13×10^{16}
Sample 3	328	37.21	0.62	7.55	1.16	84	1.10	545	2.73×10^{15}

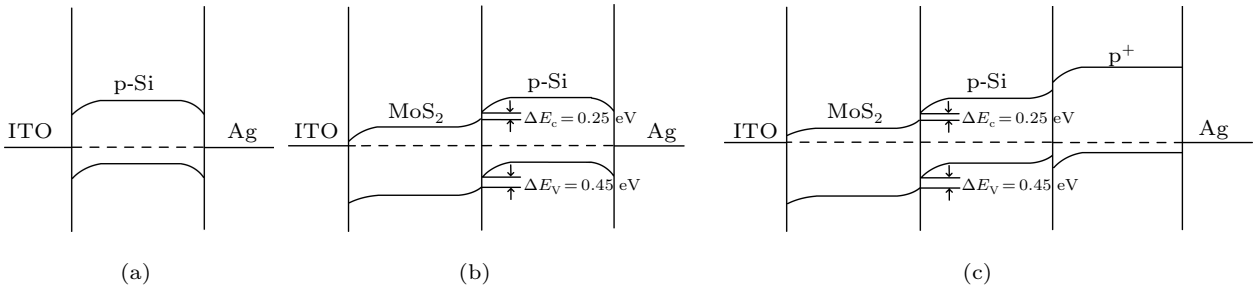


Fig. 4. Energy level diagrams of (a) sample 1, (b) sample 2, and (c) sample 3.

An energy-level diagram of sample 1 is shown in Fig. 4(a). The work functions of ITO, p-Si, and Ag are 4.5 eV, 4.9 eV, and 4.3 eV, respectively. Electron transfer from ITO to p-Si occurs at the interface between the ITO and the p-Si, forming a space region of negative charge and a Schottky barrier through the downward energy band. Similarly, a Schottky barrier is formed at the interface between the p-Si and the Ag, resulting in two back-to-back Schottky barriers. A photovoltage is generated at the ITO/p-Si Schottky junction in the measurements of the J–V curves under AM 1.5 illumination, which is equivalent to applying a positive bias voltage to the p-Si/Ag Schottky junction. The direction of the external bias voltage is opposite to that of the photovoltage, which is equivalent to applying a negative bias voltage to the p-Si/Ag Schottky junction. The external bias voltage varies continuously during the measurements. When the external bias voltage is much lower than the photovoltage, the p-Si/Ag Schottky junction is positively biased, and the positive resistance is minimal. Therefore, the effect of the Schottky junction on the current density is minimal and almost negligible. When the external bias voltage is close to the photovoltage, the forward bias voltage is too small, and the resistance cannot be ignored, resulting in a decrease in J_{SC} and the FF. V_{OC} also decreases because of the voltage divided by the p-Si/Ag Schottky junction. When the external bias voltage is higher than the photovoltage, the p-Si/Ag Schottky junction is reverse biased, and the current density approaches the reverse saturation current density with increasing external voltage, instead of increasing exponentially. Thus, the S-shaped J–V curve appears, as shown in Fig. 3(a).

Figure 4(b) shows the energy level diagram of sample 2. When ITO comes into contact with MoS_2, an electron transfer occurs from ITO to MoS_2, forming a space region of negative charge at the interface between the two layers and an ohmic contact through the downward energy band. Sample 2 is a series device which is equivalent to a p–n junction and a p-Si/Ag Schottky junction in series. The p–n junction forms a larger built-in electric field and exhibits a wider depletion region width than the ITO/p-Si Schottky junction of sample 1, which improves the V_{OC} and FF. However, the p-Si/Ag Schottky junction takes part of the voltage when the external bias voltage is close to the photovoltage, and is then reverse-biased when the external bias voltage is greater than the photovoltage. Therefore, the S-shaped J–V curve is still observed, as shown in Fig. 3(a), due to the existence of a p-Si/Ag Schottky junction.

Figure 4(c) shows the energy-level diagram of sample 3. The barrier width of the interface between the Ag and p^+ layers is relatively thin, due to the high doping concentration of the p^+ layer. Therefore, electrons can pass through the barrier region due to the tunneling effect, generating a large current and making an ohmic contact. Additionally, a high–low junction is formed between the p^+ layer and the p-Si. Consequently, the S-shaped J–V curve is eliminated, as shown in Fig. 3(a), and a higher output current density is obtained at a high voltage, compared to those of the other two solar cells.

Figure 5 presents the EQE spectra of the three samples, which show that the EQE values gradually increase. The width of the depletion region of sample 2 increases due to the introduction of the MoS_2 film, leading to an increase in the collection depth of the carriers and an improvement in the EQE.[11] An ohmic contact is formed between the p^+ layer and the Ag electrode due to the introduction of the p^+ layer, and a high–low junction is formed between the p^+ layer and the p-Si; these are more conducive to carrier transport. Therefore, the short-circuit current density is increased, and the EQE is further improved.

Figure 6 shows the C–F curves of the three samples. The high-frequency capacitance represents the response of the free carrier concentration, and the low-frequency capacitance represents the responses of both the free carrier and deep trap

concentrations.[12] In the high-frequency region, the capacitances of all the samples are almost identical, indicating that their free carrier concentrations are also nearly identical. In the low-frequency region, the capacitances of the samples gradually decrease, indicating the reduction of deep trap concentration due to the introduction of the MoS_2 film and the p^+ layer; the device performance is thus improved.

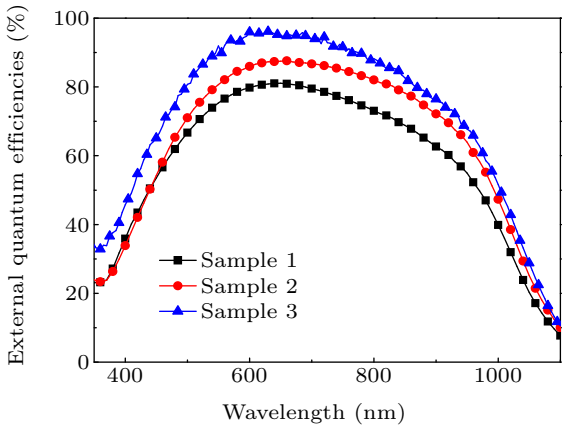


Fig. 5. EQE spectra of samples 1–3.

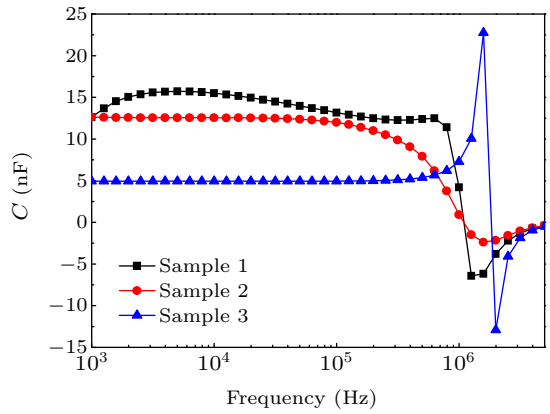


Fig. 6. The *C*–*F* curves of samples 1–3.

The C^{-2}–V curves of the three samples, as shown in Fig. 7, are measured at a frequency of 100 kHz. The C^{-2}–V curve of sample 1 is nonlinear, which indicates that the solar cell is not an abrupt junction. The C^{-3}–V curve, calculated from the C–V data, is also nonlinear, indicating that the solar cell is not a gradual junction. According to Eq. (1), for a single-sided junction, the impurity concentration (N_b) is obtained from the differential calculation of the C–V curve. The other two samples have abrupt junctions, as derived from the linear relationship of the C^{-2}–V curves. According to Eq. (2), the built-in voltage (V_{bi}) of the p–n junction is obtained from the interception of the horizontal axis.[13]

$$N_b = \frac{C^3}{qA^2\varepsilon_0\varepsilon_s}\left(\frac{dC}{dV}\right)^{-1}, \tag{1}$$

$$C = A\left[\frac{q\varepsilon_0\varepsilon_s N_b}{2(V_{bi}-V)}\right]^{1/2}. \tag{2}$$

The V_{bi} values of samples 2 and 3 are 0.93 V and 0.72 V, respectively. N_b is calculated from the slope of the C^{-2}–V curve. The values of N_b and the depletion region width (W) at $V = 0$ V are listed in Table 1, from which it can be observed that the N_b of the three samples decreases, while W gradually increases. The decrease in N_b is consistent with the results of the C–F characteristic measurements. This indicates that the introduction of the MoS_2 film and the p^+ layer reduces the impurity concentration of the solar cell. The increase in W is attributed to a decrease in the impurity concentration. The smaller value of V_{bi} and larger value of V_{OC} of sample 3, compared to those of sample 2, can be attributed to the partial voltage of the Schottky junction.

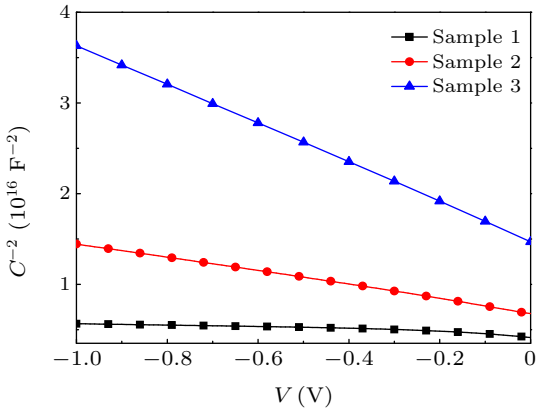


Fig. 7. The C^{-2}–V curves of samples 1–3.

4. Conclusion

In this study, the generation mechanism of the S-shaped J–V curve was analyzed by introducing a MoS_2 film and a p^+ layer into the front and back surfaces of sample 1. The depletion region width was increased by the formation of a p–n junction, and a decrease in the impurity concentration was observed to reduce carrier recombination following the introduction of the MoS_2 film, which improved the photoelectric performance of the solar cell. A high–low junction was formed between the p^+ layer and the p-Si along with an ohmic contact between the p^+ layer and the Ag electrode because of the high doping characteristics and high work function of the p^+ layer. As a result, a higher current density output was obtained at a high voltage, and the S-shaped J–V curve disappeared. Sample 3 was seen to exhibit ideal p–n junction rectification characteristics. The findings of this study may improve the application of MoS_2 thin films in the field of silicon-based solar cells, which are expected to be widely used in various silicon-based electronic and optical devices.

Acknowledgments

Project supported by the Science and Technology Research Project of Hebei Province Colleges and Universities

(Grant No. QN2020113) and Tangshan Applied Basic Research Project (Grant No. 19130227g). We would like to thank Editage (www.editage.cn) for English language editing.

References

[1] Xu H J, Xin L T, Liu L L, Pang D Q, Jiao Y X, Cong R D and Yu W 2019 *Mater. Lett.* **238** 13

[2] Xu H Y, Chen D Q, Xin L T, Xu H J and Yu W 2019 *RSC Adv.* **9** 33710

[3] Cárabe J and GandíA J J 2002 *Thin Solid Films* **403–404** 238

[4] Wang F Y, Zhang D X, Cai H K, Su C, Yu Q and Hu N 2014 *J. Synth. Cryst.* **43** 275 (in Chinese)

[5] Sims L, Hoermann U, Hanfland R, Mackenzie R C, Kogler F R, Steim R, Bratting W and Schilinsky P 2014 *Organic Electronics* **15** 2862

[6] Kim S S, Bae S and Jo W H 2015 *Chem. Comm.* **51** 17413

[7] Sapna M, Sonpal S and Vamsi K K 2018 *IEEE J. Photovolt.* **8** 909

[8] Aghassi A, Fay C D and Mozer A 2018 *Organic Electronics* **62** 133

[9] Liu Y, Bag M, Renna L A, Page Z A, Kim P, Emrick T, Venkataraman D and Russell T P 2016 *Adv. Energy Mater.* **6** 1501606

[10] Tsai M L, Su S H, Chang J K, Tsai D S, Chen C H, Wu C I, Li L L, Chen L J and He J H 2014 *ACS Nano* **8** 8317

[11] Sablon K A, Little J W, Sergeev A and Vagidov N 2012 *Vac. Sci. Technol.* **30** 04D104

[12] He B, Shi Y L and Xu J 2006 *Infrared* **27** 5 (in Chinese)

[13] Almora O, Gerling L G, Voz C, Alcubilla R, Puigdollers J and Belmonte G 2017 *Sol. Energ. Mat. Sol. C* **168** 221